HOKKAIDO UNIVERSITY

Title	Correction of the Stepwise Change Observed at 0℃ in Meisei RS2-91, RS-01G, and RS-06G Radiosonde Relative Humidity Profiles
Author(s)	Sugidachi, Takuji; Fujiwara, Masatomo
Citation	Journal of the Meteorological Society of Japan, 91(3), 323-336 https://doi.org/10.2151/jmsj.2013-306
Issue Date	2013-06
Doc URL	https://hdl.handle.net/2115/53341
Type	journal article
File Information	JMSJ91_2013-306.pdf

Hokkaido University Collection of Scholarly and Academic Papers : HUSCAP

Journal of the Meteorological Society of Japan, Vol. 91, No. 3, pp. 323–336, 2013
DOI:10.2151/jmsj.2013-306

Correction of the Stepwise Change Observed at 0°C in Meisei RS2-91, RS-01G, and RS-06G Radiosonde Relative Humidity Profiles

Takuji SUGIDACHI and Masatomo FUJIWARA

Graduate School of Environmental Science, Hokkaido University, Japan

(Manuscript received 20 August 2012, in final form 7 February 2013)

Abstract

Comparisons of relative humidity (RH) measurements between the Meisei RS-06G radiosonde and a chilled-mirror hygrometer revealed that the RS-06G radiosonde shows a stepwise change of ~3% RH at 0°C (drying when air temperature is decreasing). This is due to a discontinuous correction factor in the processing software that compensates for the temperature dependence of the RH sensor. Results from chamber experiments regarding the temperature and RH dependence of RS-06G RH sensors under steady-state conditions showed a wet bias exceeding 7% RH below ~+10°C. As this result contradicted previous in-flight intercomparisons that used the original manufacturer's correction, we investigated a possible additional dry bias caused by a thermal lag in the RH sensor. We speculated that the thermal lag of the RH sensor typically causes a dry bias during a tropospheric ascent, which largely compensates for the wet bias related to the temperature and RH dependence of the RH sensor. We observed that the experimental results of the temperature and RH dependence considering the thermal lag were in agreement with the extrapolation of the original manufacturer's correction. Consequently, we proposed to extrapolate the original manufacturer's correction, which is currently applied at temperatures between −40°C and 0°C, up to +14.5°C to resolve the artificial stepwise change at 0°C. Because the RS-06G radiosonde is a successor to the Meisei RS-01G and RS2-91 radiosondes, which have adopted the same RH sensor material installed since July 1999 and have used the same processing software, the current results should be applied to the data obtained by those radiosondes. The bias of RS-06G RH measurements using this new correction is estimated to be within 7% RH, which is within the manufacturer's specifications, being drier at +40°C and wetter between −40°C and +10°C.

Keywords humidity measurement; upper-air observation; radiosonde

1. Introduction

Relative humidity (RH) measurements from radiosondes are widely used in both operational and research applications. The Meisei RS-06G radiosonde is a successor to the Meisei RS-01G (introduced 2002) and Meisei RS2-91 (introduced 1991) rawinsonde, and it has been used operationally in Japan, Indonesia, Sri Lanka, and Taiwan. All of these models are currently in use, with the same RH sensor installed since July 1999 (Ishihara 2004), although the models have undergone changes in the sensor cap (Shimizu et al. 2008). For brevity, references in this paper to the RS-06G RH sensor also apply to the same sensor on the RS-01G and RS2-91 (only after the middle of 1999) models. During development of the balloon-borne chilled-mirror hygrometer (Sugidachi 2011), on the other hand, we used the RS-06G radiosonde and found that the RS-06G RH profiles always showed a stepwise change of ~3% RH at 0°C. Figure 1 shows an example of simultaneous soundings from the RS-06G and the cryogenic frostpoint hygrometer (CFH) (Vömel et al. 2007a), and the RS-06G RH profile shows a stepwise

Corresponding author: Takuji Sugidachi, Graduate School of Environmental Science, Hokkaido University, Sapporo, Hokkaido 060-0810, Japan.
E-mail: takuji-sugi@ees.hokudai.ac.jp
©2013, Meteorological Society of Japan

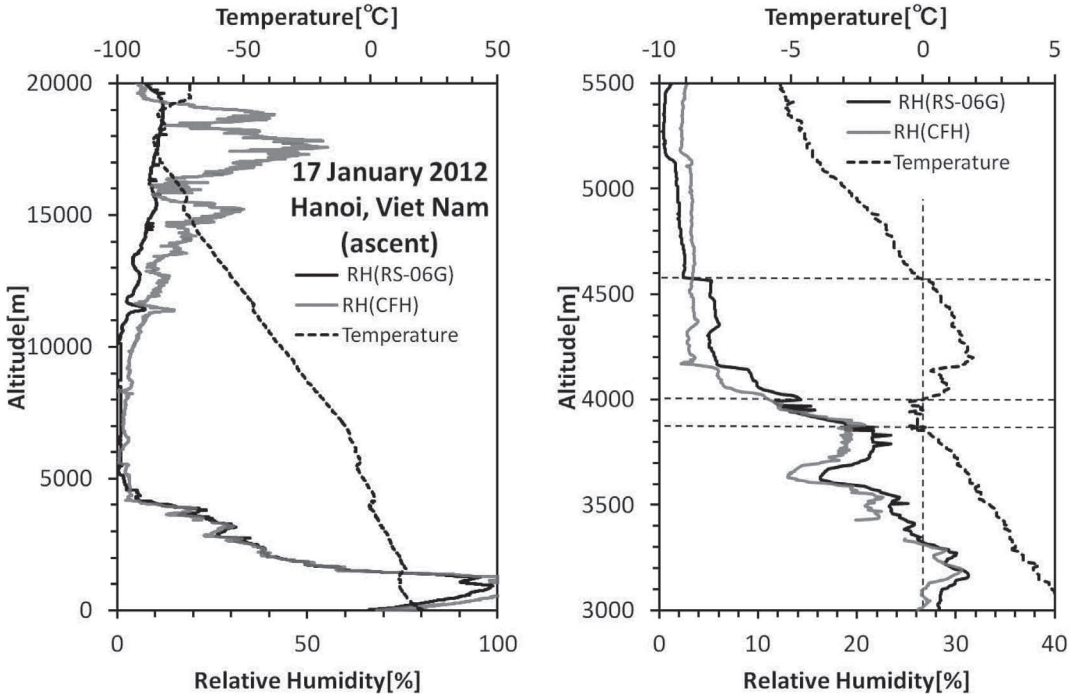

Fig. 1. Simultaneous daytime RH profiles from the Meisei RS-06G radiosonde (black) and CFH (gray) at Hanoi, Vietnam (21.01°N, 105.80°E). Dashed curves show air temperature measured with the RS-06G sensor. Left panel shows profiles for the whole troposphere, while the right panel shows the region around 0°C.

drying (wetting) of ~3% RH at 3850 m, 4000 m, and 4600 m; i.e., at 0°C air temperature, when the temperature is decreasing (increasing) through 0°C. A similar stepwise change of this magnitude is commonly observed in RS-06G RH data from other soundings.

This stepwise change is related to the correction of RS-06G RH measurements by the processing software to compensate for the temperature dependence of the RH sensor. The RS2-91 (and subsequently RS-01G and RS-06G) RH sensor is a thin-film capacitive sensor, in which a thin hydrophilic polymer layer on a glass substrate acts as the dielectric of a capacitor (Sakota et al. 1999). The capacitance changes in response to the number of water molecules permeating from ambient air into the polymer. The relationship between the capacitance and the RH of ambient air is determined by factory calibration procedures. As the individual thin-film capacitive RH sensors slightly differ, every RS2-91 (and subsequently RS-01G and RS-06G) RH sensor is calibrated in the factory at RH levels of 15%, 30%, 50%, 70%, 90%, and 95% RH at a constant air temperature of +25°C to obtain a set of instrument-specific calibration coefficients (Sakota et al. 1999). According to Ishihara (2004), RS2-91 started using a new RH sensor in July 1999, and the same sensor was used later in RS-01G and RS-06G models. After a moist bias was discovered, especially below freezing, the following temperature dependence correction has been applied, starting about February 2003, to all RH measurements at air temperatures between −40°C and 0°C obtained using these models:

$$\Delta RH = K_0 + K_1 T + K_2 T^2$$
$$RH_{\mathrm{corr}} = RH_0 - \Delta RH$$
$$(-40^{\circ}\mathrm{C} \leqq T \leqq 0^{\circ}\mathrm{C}) \qquad (1)$$

where ΔRH (%) is the correction amount, T (°C) is the air temperature uncorrected for solar heating, RH_0 (%) is the uncorrected RH, RH_{corr} (%) is the corrected RH, and K_i is a constant (K_0 = 2.86, $K_1 = -1.68 \times 10^{-1}$, $K_2 = -2.02 \times 10^{-3}$). While the Japan Meteorological Agency (JMA) only officially reports radiosonde RH measurements above −40°C, in RS-06G RH measurements for research applications, the correction in Eq. (1) is further extrapolated to below −40°C (Meisei 2012, personal communication). The largest correction factor is 6.4% RH at −40°C, and the smallest is 2.86% RH at 0°C. Therefore, the correction has a finite value of 2.86% RH at 0°C, causing an artificial stepwise

change of ~3% RH at 0°C, as shown in Fig. 1. Although the manufacturer claims that the accuracy of the RS-06G is 7% RH, this correction for the temperature dependence produces an unrealistic stepwise change at a key atmospheric level, the 0°C level, and this requires revision.

The atmospheric 0°C level (~3 km in mid-latitudes and ~5 km in the tropics) is the melting layer, where falling ice particles or snowflakes become liquid water (Houze 1993). This melting layer is important for precipitation processes and cloud dynamics. In radar meteorology, the melting layer is known as the bright band, and it produces intense radar echoes. Although atmospheric characteristics can significantly change at the 0°C level, the stepwise change of ~3% RH obtained using the RS-06G RH sensors is not realistic but is artificially generated as explained above. In this study, we investigate the temperature and RH dependence of the RS-06G RH sensor in a chamber for developing a more appropriate correction curve that is continuous at 0°C.

In general, thin-film capacitive RH sensors may be subject to several other sources of error, depending on the manufacturer and model of radiosondes, including a slow sensor response at low temperatures, contamination errors caused by supercooled cloud droplets, bias errors related to non-water molecules being absorbed into the hydrophilic polymer layer, and dry bias errors due to differences between the RH sensor temperature and the ambient air temperature caused by a thermal lag of the RH sensor during radiosonde ascent and by solar heating during daytime flights (e.g., Wang et al. 2002; Miloshevich et al. 2001; Vömel et al. 2007b; Yoneyama et al. 2008). Among these errors, the thermal lag of the RH sensor is caused by the finite time required for RH sensors to reach equilibrium with the changing ambient air temperature during flight (e.g., Morrissey and Brousaides 1970; Williams and Acheson 1976; WMO 2008). In this study, we also investigate the thermal lag of the RS-06G RH sensor using a laboratory-based thermostatic chamber test.

The remainder of this paper is organized as follows. Section 2 describes two experiments, and their results, which test the temperature dependence and thermal lag of the Meisei RS-06G RH sensor. Section 3 proposes a new correction for RS-06G RH measurements based on results from these two experiments and provides an example of the application of the new correction. Section 4 provides a summary and concluding remarks.

2. Experiments

2.1 Estimation of temperature dependence between −50 and +40°C

We estimated the temperature dependence of 10 RS-06G RH sensors by comparing them with reference instruments under various chamber conditions, at air temperatures from −50 to +40°C, and at RH levels from 20% to 80% (The Ishihara (2004) correction was derived using tests in a similar chamber). We built a special experimental setup for this experiment. Figure 2 shows the overall configuration of this experiment. Five RS-06G RH sensors and reference sensors were placed in a polyvinyl chloride (PVC) pipe with an inner diameter of 65 mm, which was then placed in the thermostatic chamber (Espec PSL-4KH). This chamber can control temperature between −70 and +150°C and humidity within 20–98% RH above ~+10°C. The internal volume of the chamber is 800 l. An RF-100 platinum resistance thermometer (Electric Temperature Instruments (ETI)) was used as a reference temperature sensor, and the FDW10 chilled-mirror hygrometer (Azbil Corporation; Ibata and Kanai 2008) was used as a reference dew point sensor (see Table 1 for the manufacturer's specifications for these instruments). An airflow of about 2 m s^{-1} was produced within the pipe using a fan located at its entrance to ensure uniformity in the measurement air. Two sets of five RS-06G RH measurements were made. As stated in note (1) in Table 1, the first set of five radiosondes represented four manufacturing batches, and the second set of radiosondes was from the same batch. Figure 3 (bottom) shows the temperature and RH conditions for all measurements in this experiment. RH values are with respect to liquid water, and no experiments were performed with RH values supersaturated with respect to ice. For each set, the RH and temperature in the chamber were changed every 30 to 60 minutes under surface pressure conditions (~1000 hPa) to ensure a steady measurement condition. This made it possible to ignore errors derived from the slow sensor response and the thermal lag of the RH sensor. Readings were taken five times every 10 to 20 s for each set of conditions.

We analyzed the data that are not corrected using Eq. (1) (hereinafter referred to as "RS-06G RH_0"). We calculated the reference RH values from the reference temperature and reference dew point readings using Buck's equations (Buck 1981; Appendix A), which is also used for the RS-06G calibration by the manufacturer (WMO 2011; Meisei 2012, personal communication). In the upper air observation, RH is

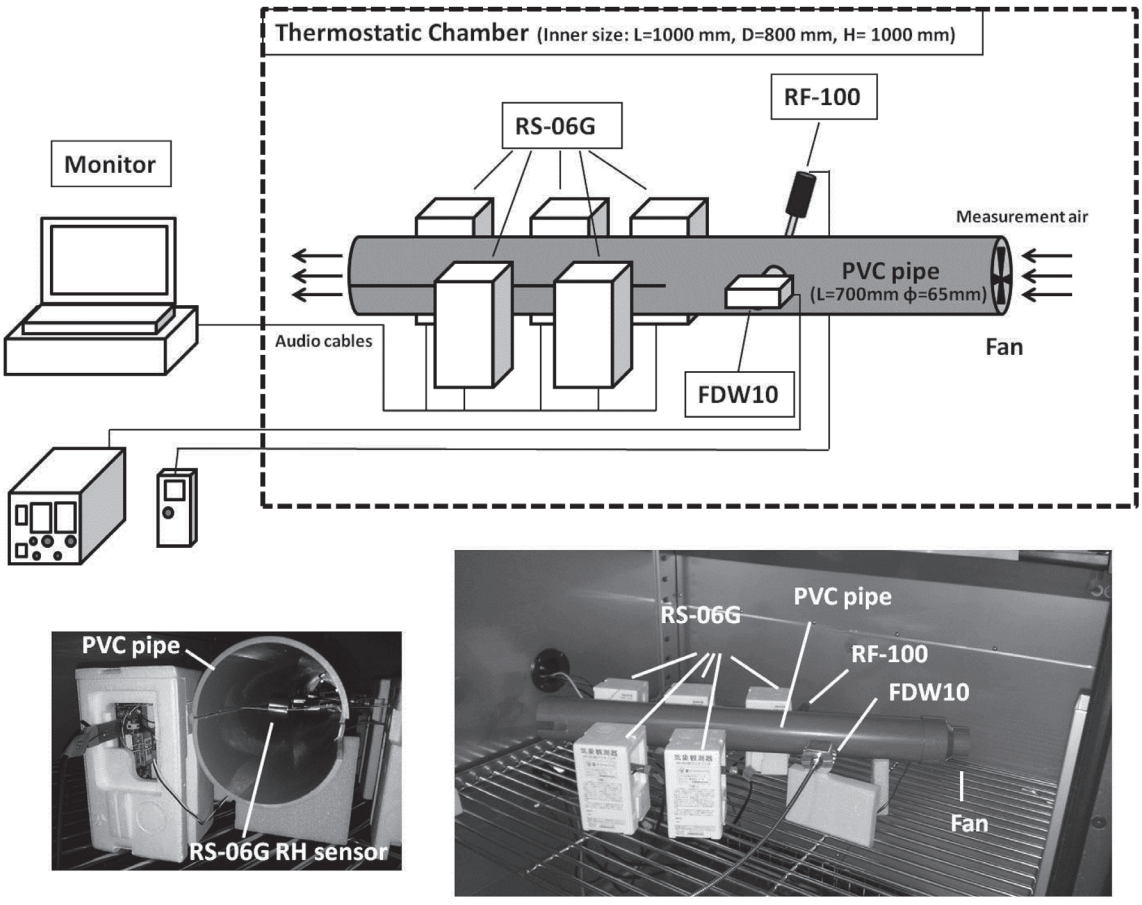

Fig. 2. Experimental setup in the thermostatic chamber. The bottom left picture shows the sensor probe of RS-06G in the PVC pipe. The bottom right picture shows the five RS-06G radiosondes and the two reference instruments set in the PVC pipe.

Table 1. Manufacturer's specification details for the instruments.

	RS-06G[1)]		FDW10	RF-100
	thermometer	hygrometer		
Manufacturer	Meisei	Meisei	Azbil Corporation	ETI
Principle	thermistor	thin-film capacitive sensor	chilled mirror hygrometer	platinum thermometer (PT100)
Range	−90°C to +40°C	1 to 100% RH	−40 to +100°C DP[2)]	−199.9 to +199.9°C
Resolution	0.1°C	0.1% RH	0.1°C DP	0.01°C
Accuracy	±0.5°C (2σ)	±7% (2σ)	±0.5°C DP	±0.05°C (−30°C to +150°C) ±0.1°C (other conditions)

1) Serial numbers (and the sensor age, months after the production date) of radiosondes used in the experiment are 100261 (0 months), 100262 (0 months), 100270 (9 months), 100977 (5 months), 101587 (2 months), 102259 (0 months), 102260 (0 months), 102261 (0 months), 102262 (0 months), and 102263 (0 months).

2) °C DP represents dew/frost point temperature.

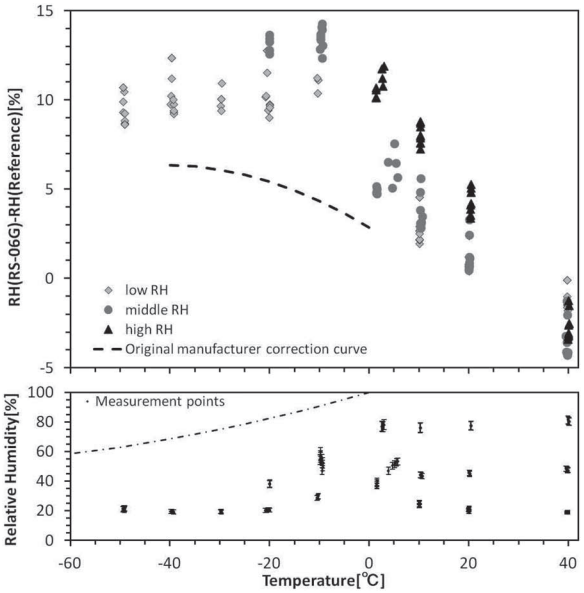

Fig. 3. (top) Temperature dependence of RS-06G RH measurements under different RH conditions. The RH difference between the reference and the uncorrected RS-06G RH_0 is indicated by gray squares (for <30% RH), dark gray circles (for 30% to 70% RH), and black triangles (for >70% RH). The dashed curve represents the original manufacturer's correction curve. (bottom). Dots represent the experimental conditions and vertical bars represent uncertainties. The dot–dashed curve in the bottom panel indicates ice saturation.

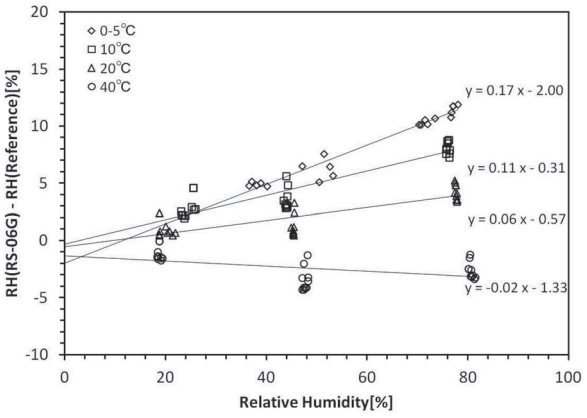

Fig. 4. RH dependence of the RS-06G RH measurements under different temperature conditions. The RH difference between the reference and the uncorrected RS-06G RH_0 is indicated by rhomboids (for 0 to +5°C), squares (for +10°C), triangles (for +20°C), and circles (for +40°C). The lines are linear fits for each temperature group.

usually evaluated with respect to liquid water even at air temperatures below 0°C (WMO 2008). Accordingly, if the condensate on the mirror of the FDW10 is liquid water,

$$RH = 100\frac{e_w(T_m)}{e_w(T_a)} \tag{2}$$

where e_w is the saturation vapor pressure of moist air with respect to water, T_m is the mirror temperature, and T_a is the air temperature. If the condensate on the mirror of the FDW10 is ice,

$$RH = 100\frac{e_i(T_m)}{e_w(T_a)} \tag{3}$$

where e_i is the saturation vapor pressure of moist air with respect to ice.

The measurement uncertainties associated with these experiments are expressed according to the Guide to the Expression of Uncertainty in Measurement (GUM) (JCGM/WG1 2008). Conceivable measurement uncertainties in the reference RH are derived from the instrument performance, errors in reading, and spatial and temporal non-uniformity in the PVC pipe. The combined standard uncertainties are calculated from these sources of uncertainty. The error bars in Fig. 3 represent the 95% level of confidence (the coverage factor k = 2). The expanded uncertainties of the reference RH level range between 0.7% and 3.2% RH. Meanwhile, the five readings of RS-06G RH_0 values are closely comparable, with typical standard deviation of ~0.1% RH, an order of magnitude smaller than the measurement uncertainty of the reference RH. The error bars for the RS-06G RH_0 values are omitted in Fig. 3. The calculation of the measurement uncertainties is described in detail in Appendix B.

Figure 3 shows the difference between the RS-06G RH_0 and the reference RH values at each temperature and RH condition for all measurements. The values of RS-06G RH_0 are wetter than the original manufacturer's correction factor (dashed line in Fig. 3) by 7% RH or more for some conditions below +10°C. Figure 4 shows the difference between RS-06G RH_0 and the reference RH with respect to RH. It shows that RS-06G RH_0 has an RH dependence in addition to temperature dependence. These biases can be approximated by a linear regression between 20% and 80% RH. The wet bias is greater in wetter conditions when air temperatures are below +20°C. The wet bias approaches 10% RH at high RH and low-temperature

conditions. In contrast, a small dry bias is found at +40°C. From these results, the RS-06G RH_0 levels show a tendency toward a dry bias above about +25°C, and a wet bias below about +25°C. It should be noted again that the temperature of +25°C is the calibration condition used by the manufacturer. These results, the large bias of over 7% RH and the RH dependence, are surprising and will be further explored in the next section.

2.2 *Estimation of thermal lag for the RS-06G RH sensor*

Figure 3 showed that our measured values of RS-06G RH_0 were significantly different from the original manufacturer's correction curve, exceeding 7% RH under some conditions. However, such a large bias was not reported for in-flight intercomparisons with other radiosonde models (e.g., WMO 2011). We believe that this discrepancy arises because of differences in measurement conditions; i.e., in a chamber or in flights. Here we focus on the difference in air temperature conditions; air temperatures in our chamber experiments were stable by experimental design, while air temperatures in flights can dramatically change over a short period. If the thermal lag of the RH sensor is not negligible, the RH sensor temperature will not immediately correspond to the ambient air temperature. During an ascending flight through the troposphere, the RH sensor temperature would usually be warmer than the ambient air temperature. The warmer RH sensor would result in RH measurement results with a dry bias. Therefore, there is a possibility that RS-06G RH measurements always have a dry bias component in the troposphere. It should be noted that the RS-06G RH sensor is mounted in a sensor hood to minimize solar heating effects and contamination by supercooled cloud droplets and rain.

To estimate the dry bias component caused by the thermal lag of the RS-06G RH sensor, we investigate the response time of the RH sensor temperature to a stepwise air temperature change in a chamber. A thermistor, which is used as an air temperature sensor of the RS-06G, was used to measure the RH sensor temperature. The thermistor has a negligible heat capacity with a response time of 1.3 s at 1000 hPa even without airflow (Shimizu et al. 2008). Furthermore, the use of the same type of thermistors for the RH sensor and air temperatures minimizes error in the thermal lag evaluation. The thermistor was attached to the surface of the RH sensor using aluminum tape whose heat capacity is also sufficiently small. We measured the response time in the chamber as the air temperature was changed from 0°C to +10°C over a short period of around 100 s. This experiment was conducted under the following three conditions:

(1) without the sensor hood;

(2) with the sensor hood, and in an airflow perpendicular to the sensor arm; and

(3) with the sensor hood, and in an airflow parallel to the sensor arm.

The airflow was ~3 m s^{-1} for all conditions. The sensor in flights is usually exposed to a stronger airflow than these conditions, because the ascent rate of the radiosonde is usually set as ~6 m s^{-1}. However, we cannot replicate the flight condition of the radiosonde because of experimental constraints. Specifically, the maximum wind speed by the fan we used is ~3 m s^{-1} at ~1000 hPa. Also, it is impossible for us to control the airflow under reduced pressure conditions. Thus, we conducted this experiment only under surface pressure and estimated the thermal lag in ascent flight using these experimental results and some assumptions.

Figure 5 shows the response time of the RH sensor temperature, T_s, and the applied measurement condition, T_a. On the basis of Newton's law of cooling, the relationship between T_s and T_a can be written as

$$\tau \frac{dT_s(t)}{dt} + T_s(t) = T_a \tag{4}$$

where τ is the time constant. By replacing $dT_s(t)/dt$ with $(T_s(t) - T_s(t - \delta t))/\delta t$, where δt is a finite time step, $T_s(t)$ is solved as

$$T_s(t) = \frac{T_a \delta t + \tau T_s(t - \delta t)}{\tau + \delta t} \tag{5}.$$

Figure 5 also shows the estimated RH sensor temperature, T_{s_est}, profile derived from Eq. (5) with a constant τ for each experiment; i.e., 10 s in Fig. 5(1), 25 s in Fig. 5(2), and 50 s in Fig. 5(3). We see that the assumed value of τ explains the evolution of T_s reasonably well.

We also estimate the thermal lag of the RH sensor during actual flights. The thermal lag should depend on the heat transfer between the ambient air and the surface of the RH sensor. As air density decreases with height, the temperature difference between the ambient air and the RH sensor is expected to increase at higher altitudes. Williams and Acheson (1976) theoretically express the time constant, τ, as

$$\tau = \frac{mc}{hA} \tag{6}$$

where m is the mass of the sensor, c is the specific heat,

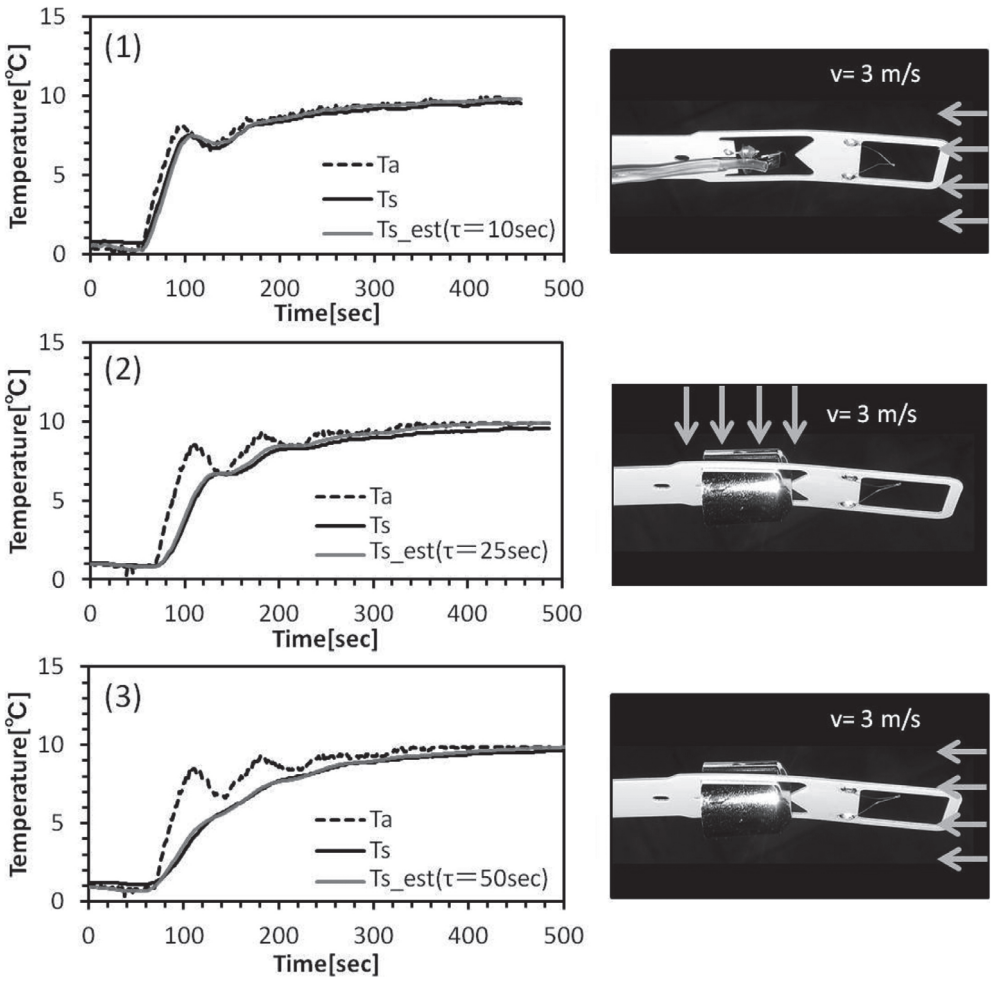

Fig. 5. Temperature profiles of the RS-06G RH sensor in response to a stepwise change in air temperature in a chamber (left), and a photo showing the three different measurement conditions (right). Dashed lines show applied air temperature, black lines show the change in the sensor's surface temperature, and gray lines show estimated sensor temperatures; i.e., air temperature data filtered with Eq. (5) using the indicated τ value.

h is the convective heat-transfer coefficient, and A is the total surface area of the sensor. Morrissey and Brousaides (1970) proposed that, assuming that the RH sensor is a flat plate with a zero angle of attack to airflow, h can be calculated from

$$h = \frac{1}{L}\int_0^L 0.332 k Pr^{\frac{1}{3}} \left(\frac{\rho v'}{\mu x}\right)^{\frac{1}{2}} dx \tag{7}$$

where L is the width of the RH sensor, k is the thermal conductivity of air, Pr is the Prandtl number, ρ is the density of air, v' is the flow rate on the RH sensor, and μ is the viscosity coefficient. The values of Pr, k, and μ depend on air temperature. For the RS-06G RH sensor, v' is not equal to the ascent rate v because of the sensor hood and the irregular payload movement during flight. Here, we assume that v' is proportional to v, that is,

$$v' = Cv \tag{8}$$

where C is a constant that indicates the effect on how the ventilation changes by the sensor hood and airflow direction. Substituting Eqs. (7) and (8) into Eq. (6), τ can be rewritten as

$$\tau = C' k^{-1} Pr^{-\frac{1}{3}} \left(\frac{\mu}{\rho v}\right)^{\frac{1}{2}} \tag{9}$$

where C' is a constant depending on the RH sensor property and the C value. To estimate τ during actual

flights, we calculate the C' value by using the time constant obtained from the chamber experiment (Fig. 5). It is considered that the sensor hood may cause poorer ventilation, while the pendulum motion of the payload during ascent flights may cause better ventilation. We assume that the condition without the sensor hood [i.e., Fig. 5(1)] is the best-ventilated condition, because nothing blocks the airflow. On the other hand, we assume the condition with the sensor hood and in an airflow parallel to the sensor arm [i.e., Fig. 5(3)] as the worst-ventilated condition, because the sensor hood substantially obstructs the airflow. Given these assumptions, it is considered that the actual flight condition lies between the conditions in Fig. 5(1) and 5(3), i.e., we use the results from Fig. 5(1) and 5(3) as the upper and lower limits, respectively. The C' values become 102 kg $m^{\frac{1}{2}}$ s^{-2} K^{-1} for Fig. 5(1), and 512 kg $m^{\frac{1}{2}}$ s^{-2} K^{-1} for Fig. 5(3). Assuming that the possible value of C' at the flight condition is probable between these values (i.e., a rectangular distribution), the expected C' value is the midpoint of the interval, 307 kg $m^{\frac{1}{2}}$ s^{-2} K^{-1}. Then, the standard uncertainty, $u_{C'}$ is

$$u_{C'} = \frac{512 - 102}{2\sqrt{3}} = 118 \text{ kg m}^{\frac{1}{2}} \text{ s}^{-2} \text{ K}^{-1} \quad (10)$$

Also, we estimate τ during actual flights with an ascent rate of 6.0 ± 1.0 m s^{-1}. While the ascent rate of the radiosonde is usually set at ~6 m s^{-1}, the value may vary according to the meteorological condition by ~1.0 m s^{-1} even in the troposphere. The standard uncertainty from the ascent rate fluctuation, u_v, is

$$u_v = \frac{1}{\sqrt{3}} = 0.58 \text{ m s}^{-1} \quad (11)$$

Using this C' value, the ascent rate of 6.0 ± 1.0 m s^{-1} and the atmospheric profile from the U. S. standard atmosphere (NOAA, NASA, and USAF 1976), we calculate τ and the temperature difference between the RH sensor and the ambient air, ΔT, in the upper air (considering only the lag error of temperature response of the sensor substrate, not other errors mentioned above such as solar heating in daytime).

Finally, we estimate the uncertainty of τ using the law of propagation of uncertainty. The combined standard uncertainty of τ, u_τ, is written as

$$u_\tau = \sqrt{\left(\frac{\partial \tau}{\partial C'}\right)^2 u_{C'}{}^2 + \left(\frac{\partial \tau}{\partial v}\right)^2 u_v{}^2} \quad (12)$$

To determine the expanded uncertainty, we use $k = 2$ as a coverage factor. Thus, the expanded uncertainty of RH, U_τ, becomes

$$U_\tau = k u_\tau = 2 u_\tau \quad (13)$$

Figure 6 shows the air temperature and density profiles from the U. S. standard atmosphere and the calculated values of τ and ΔT. The light and dark gray lines show the expanded uncertainties estimated by Eq. (13). This figure suggests that ΔT is larger at higher altitudes; e.g., 0.9 ± 0.7°C at 5 km and 1.3 ± 1.0°C at 10 km. The RH sensor that is warmer because of the thermal lag indicates a RH drier than the actual RH, because the saturation vapor on the surface of the RH sensor is not $e(T_a)$ but $e(T_a + \Delta T)$, i.e.,

$$RH_{flight} = 100 \frac{e}{e_w(T_a + \Delta T)} \quad (14)$$

where RH_{flight}, is the RH obtained from the RS-06G in flight, and e is the vapor pressure of measurement air. On the other hand, the RH in a chamber, $RH_{chamber}$, is calculated by Eq. (2) or (3). Accordingly, the relationship between $RH_{chamber}$, and RH_{flight} is

$$RH_{chamber} = RH_{flight} \times \frac{e(T_a + \Delta T)}{e(T_a)} \quad (15).$$

When $\Delta T > 0$, RH_{flight} is drier than $RH_{chamber}$. Because the RS-06G RH sensor becomes $\Delta T > 0$ in tropospheric ascents as shown in Fig. 6, it is considered that the thermal lag could cause dry bias for the RS-06G RH measurements.

3. A new correction for RS-06G RH measurements

The results of these two experiments show that the RS-06G RH_0 value has a wet bias component caused by the temperature and RH dependence of the sensor material and a dry bias component related to the thermal lag of the RH sensor, which is warmer than the ambient air temperature during a tropospheric balloon ascent. It is expected that the two biases are, at least in part, canceled out during a flight, and the measurement accuracy of 7% RH (k = 2) proposed by the manufacturer is achieved. To fully characterize the sensor's behavior in flight and to obtain a complete correction algorithm, we need to consider all other measurement errors, in addition to the two biases outlined above. Major errors include the slow response of the RH sensor at low temperatures (Miloshevich et al. 2004), and the solar heating dry bias (Vömel et al. 2007b; Yoneyama et al. 2008). Consequently, herein, we propose a simple correction to remove the artificial stepwise RH change at 0°C that results from the use of Eq. (1). We assume that the two biases discussed in

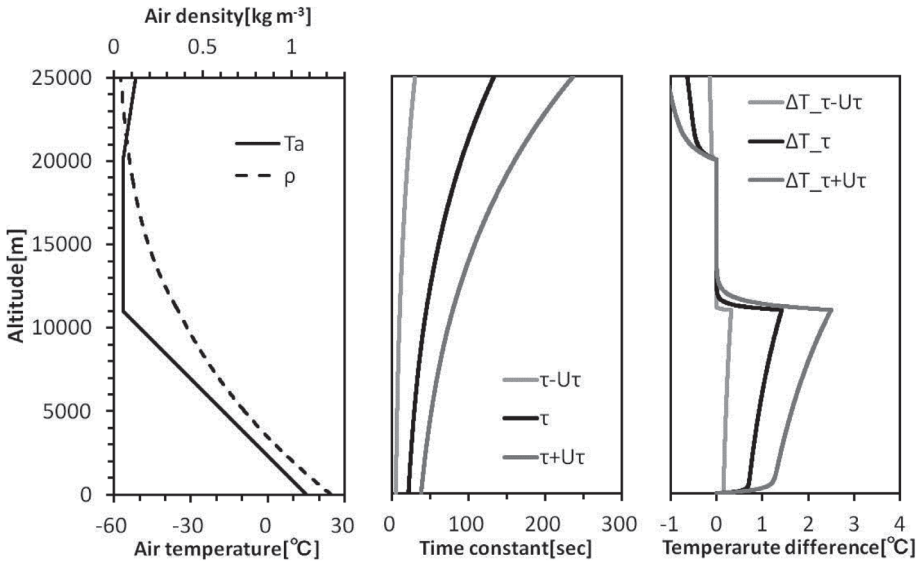

Fig. 6. (left) Temperature and density profiles from the U.S. standard atmosphere. (center) The time constant calculated by Eq. (9). The black line indicate the value derived from C' = 307 kg $m^{\frac{1}{2}}$ s^{-2} K^{-1}. The light and dark lines indicate the expanded uncertainties, i.e., $\tau - U_\tau$ and $\tau + U_\tau$. The difference between the RH sensor temperature and ambient air temperature for the three conditions.

Section 2 are the major sources of error. As a test, we add the dry bias component to the wet bias component shown in Fig. 3. Using the relationship of Eq. (15), the correction factor during tropospheric ascents then becomes

$$\Delta RH = RH_{flight} - RH_{ref} = RH_0 \times \frac{e(T_a)}{e_w(T_a + \Delta T(T_a))} - RH_{ref} \quad (16).$$

Although $\Delta T(T_a)$ depends on the actual vertical gradients of air temperature and air density and the ascent rate of the radiosonde, we use the results in Fig. 6 for simplicity. Figure 7 shows $\Delta T(T_a)$ and corresponding linear fits. Figure 8 shows the RH difference between the reference RH and the corrected value by applying the correction for the thermal lag expressed by Eq. (16). Figure 8 also shows the original manufacturer's correction curve extrapolated up to +14.5°C. The upper limit of +14.5°C is chosen, because the original manufacturer's correction curve intersects ΔRH = 0 at + 14.5°C. The marks in the figure indicate the value derived from ΔT_τ in Fig. 7, and the light gray vertical bars indicate the uncertainties derived from $\Delta T_\tau \pm U_\tau$ in Fig. 7. We see that the corrected experimental results and the extrapolated correction curve show a better agreement above 0°C,

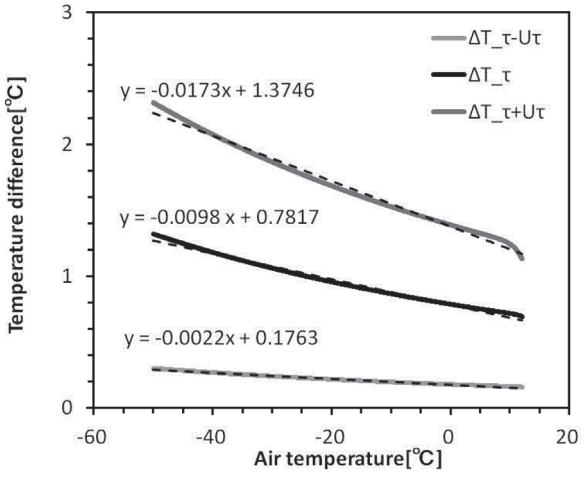

Fig. 7. Temperature difference shown in the right panel of Fig. 6 against the ambient air temperature shown in the left panel of Fig. 6. Dotted lines show the linear fit.

as well as below 0°C. Consequently, we propose to extrapolate the original manufacturer's correction up to +14.5°C to resolve the artificial stepwise change at 0°C. Extrapolating the correction above +14.5°C to

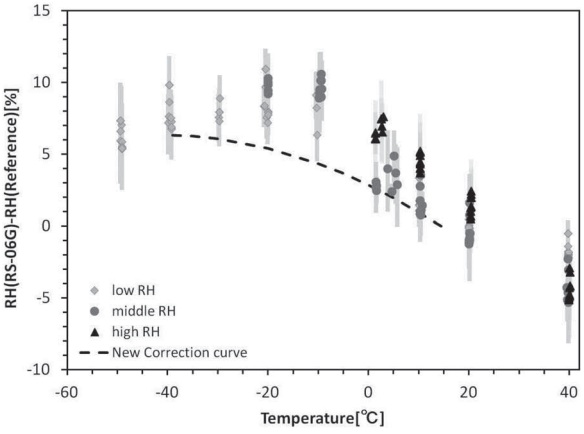

Fig. 8. As in Fig. 3 (top), but corrected by Eq. (16) for a modeled thermal lag effect. The dashed line represents the correction curve extrapolated up to 14.5 + ˚C. Vertical light gray bars represent the estimated magnitude of uncertainty from the thermal lag effect. The marks indicate the value derived from $C' = 307$ kg $m^{\frac{1}{2}}$ s^{-2} K^{-1}, and the upper and lower limits of the light gray vertical bars indicate the uncertainty derived from Eq. (13).

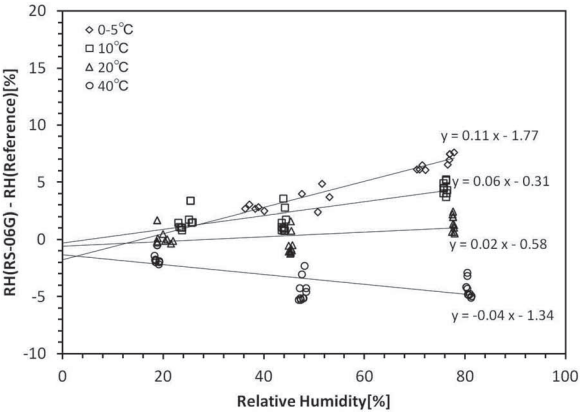

Fig. 9. As in Fig. 4, but corrected by Eq. (16) for a modeled thermal lag effect.

adjust for the dry bias at higher temperatures (Fig. 8) is not recommended, because biases with a zero correction, even at 40˚C, are within specifications.

In addition, we observed that the RS-06G RH_0 value has an RH dependence, as shown in Fig. 4. Equation (16) is effective at reducing the bias associated with the RH dependence below +20˚C. Figure 9 shows the difference between the RS-06G RH_0 corrected by Eq. (16) and the reference RH with respect to RH and the corresponding linear fit. The RH dependence corrected by Eq. (16) (i.e., Fig. 9) is smaller than in the uncorrected result (i.e., Fig. 4), except at +40˚C.

Figure 10 shows the estimated bias in the RS-06G RH measurements during a tropospheric balloon ascent, that is, the result of subtracting the proposed correction amount from the results in Fig. 8. The error bars in Fig. 10 show the uncertainty (k = 2), including that from the dry bias estimation, that from the reference RH in our chamber experiment, and that from the individual differences of the RS-06G RH sensor. Each component of the uncertainty (k = 2) is estimated as 0.3% to 3.8% RH for the dry bias estimation, 0.7% to 3.3% RH for the reference RH, and 0.3% to 0.9% RH for the individual differences among the 10 sensors (two times the standard error). We find that the differences among the individual RS-06G RH sensors are very small. Figure 10 indicates that there

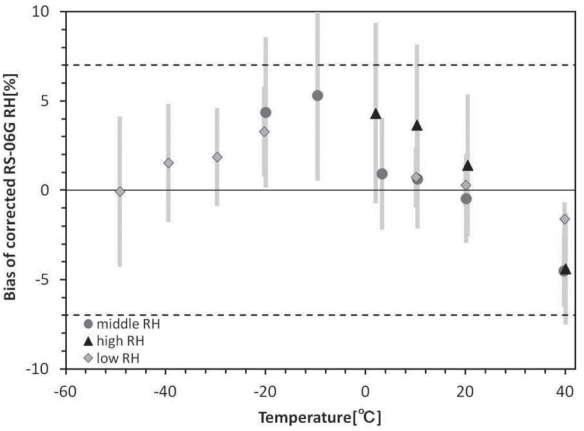

Fig. 10. Expected biases in the RS-06G RH measurements during a tropospheric balloon ascent based on the temperature and RH dependence of the sensor material and the thermal lag of the RH sensor. The results are indicated by gray squares (for <30% RH), dark gray circles (for 30% to 70% RH), and black triangles (for >70% RH) show that there remains a wet bias (<5% RH) at −40 to +10˚C. Vertical light gray bars represent the uncertainty (k = 2). Dashed lines show ±7% RH, which indicate the manufacturer's specifications.

remains a wet bias (<5% RH) at −40 to +10˚C, but these biases are within 7% RH, which is the manufacturer's specification. For daytime flights, solar heating is expected to cause an additional dry bias component. The RH profiles from the RS-06G in the World Meteorological Organization (WMO) radio-

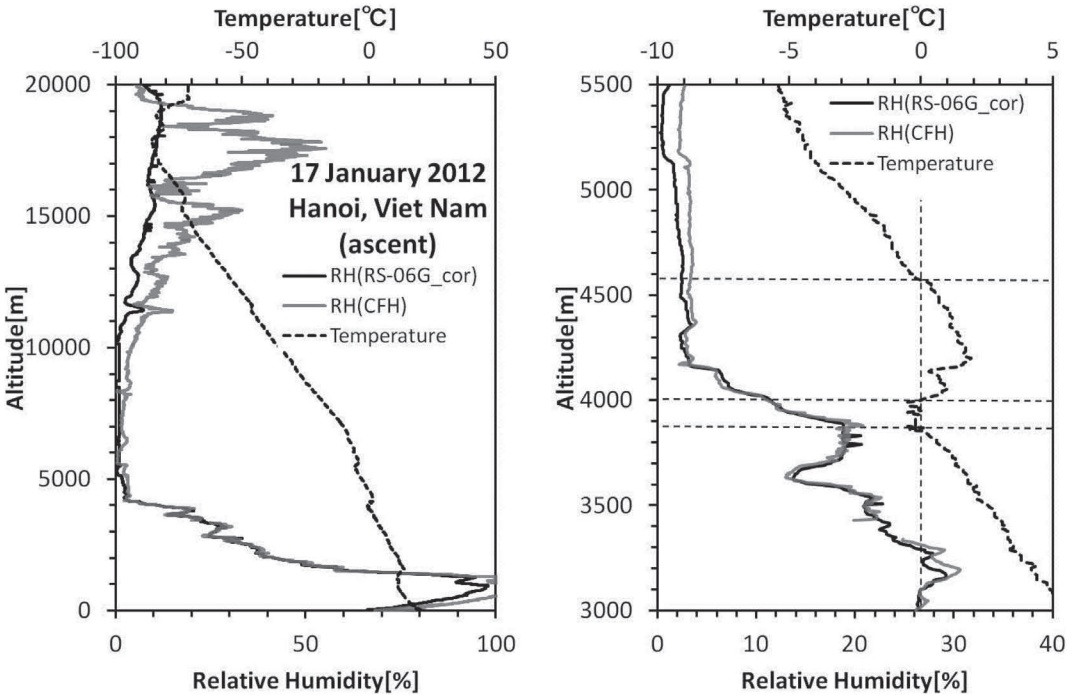

Fig. 11. As in Fig. 1, but for the RS-06G RH profiles with the new correction applied.

sonde intercomparison campaign at Yangjiang in 2010 showed day-night differences (Figure 8.2.5, lower left, of WMO, 2011). The nighttime intercomparison results in WMO (2011) showed that the RS-06G RH measurements are ~5% RH higher than the CFH measurements in the middle troposphere; this is quantitatively consistent with our experiment results in Fig. 10. Meanwhile, the daytime intercomparison results in WMO (2011) showed that the RS-06G and CFH RH measurements agree within ~3% RH in the middle troposphere; this can be interpreted that during the daytime, an additional dry bias by solar radiation heating accidentally cancels out the wet bias at −40 to +10°C shown in Fig. 10.

Figure 11 shows the RH profile from Fig. 1 corrected using our new simple approach, and it shows that the stepwise change in RH has been eliminated.

4. Summary and concluding remarks

The stepwise change in the Meisei RS-06G RH measurements at 0°C (drying when air temperature is decreasing) is caused by a discontinuity in the original manufacturer's correction algorithm, which is used to compensate for the temperature dependence of the RH sensor. We re-estimated the temperature and RH dependence of the RS-06G RH sensors in laboratory experiments and found wet biases exceeding 7% RH that had not been found in past in-flight intercomparisons. We further investigated a dry bias component caused by the thermal lag of the RH sensor. We speculated that these two biases significantly cancel each other out during tropospheric flights, and the accuracy of ±7% RH claimed by the manufacturer is achieved. We saw that the experimental results of the temperature and RH dependence considering the thermal lag agreed with extrapolating the original manufacturer's correction above and below 0°C. Consequently, we proposed to extrapolate the original manufacturer's correction up to +14.5°C to resolve the artificial stepwise change at 0°C. The remaining biases of the corrected RS-06G RH are generally within 7% RH, with small wet biases at −40 to +10°C and small dry biases at +40°C. In addition, solar heating may cause an additional dry bias of 5%–10% RH on daytime flights that would shift the obtained RH values even closer to the true RH below ~+10°C.

The new correction should be applied to the RH measurements using the RS2-91 (only after the middle of 1999), RS-01G, and RS-06G radiosondes at least

until the development of a more accurate correction. Operational soundings made with RS2-91, RS-01G, and RS-06G radiosondes are identified in text format soundings by instrument codes 47, 55, and 30, respectively, in the 31313 section (Code Table 3685 in WMO, 1995). For users of either current or archived soundings, perform the following steps:

(1) From the 31313 section of the original sounding (usually reported in part TTBB, or possibly several sounding parts), if the instrument and sounding system codes are 74702, 55504, 55508, 75508, or 73008, continue to step 2. Besides most Japanese stations, this includes 12 stations in Indonesia, 1 station in Sri Lanka, and 2 stations in Taiwan reporting one or more of the above codes starting between 2004 and 2010 (Aerological Observatory 2012, personal communication; Meisei 2012, personal communication). If the 31313 section is completely omitted or is any other value, it is unlikely that the RS-06G humidity sensor is used.
(2) If the code is 74702 (RS2-91), the old humidity sensor is used before July 1999 at JMA stations and before about the beginning of 2000 at stations 47580 and 47681 (Japanese Self-Defense Forces stations) and 89532 (Syowa, Antarctica) (Schroeder 2008). If the new sensor is used, continue to step 3. None of the corrections in this paper apply to the old humidity sensor.
(3) At any station except 47991 before approximately February 2003 (station 47991 before August 2003), the new sensor is used with no correction. Apply the manufacturer correction (1) at all temperatures up to +14.5°C.
(4) After the date in step 3, the correction is applied up at temperatures up to 0°C; thus, apply (1) at all temperature levels from +0.1 to +14.5°C to eliminate the RH discontinuity.

Of the errors affecting RH sensors listed in the introduction, this study addresses calibration errors from the inaccurate temperature and RH dependence of the sensor material and dry bias from the lag of temperature change of the sensor substrate during flight. Since the thermal lag depends on actual flight conditions, further studies of actual flights are required. In addition, other error sources should be considered to develop a more accurate correction.

Acknowledgments

Laboratory experiments were conducted using the facilities of Meisei Electric Co., Ltd. The RS-06G radiosondes were provided by Meisei Electric Co., Ltd. The use of the FDW10 was supported by Azbil Corporation. We thank the Soundings of Ozone and Water in the Equatorial Region (SOWER) project for providing Hanoi sounding data. We also thank two anonymous reviewers and Dr. Hisashi Abe of the National Metrology Institute of Japan for providing useful comments and suggestions, and the JMA Aerological Observatory and Meisei Electric Co., Ltd. for providing information about operational soundings. This study was in part supported by the Japanese Ministry of Education, Culture, Sports, Science and Technology (MEXT) through a Grant-in-Aid for Scientific Research (22740306), and the Institute of Space and Astronautical Science/Japan Aero-space Exploration Agency (ISAS/JAXA).

Appendix A

Several equations exist for the vapor pressure of water or ice (Murphy and Koop 2005). Here we use Buck's equations (Buck 1981), because they are used by the manufacturer to calibrate the RS-06G sensor. Buck's equations are written as

$$e_w = f_w \times 6.1121 \exp\left(\frac{17.502T}{240.97+T}\right) \quad \text{(A.1)}$$

$$e_i = f_i \times 6.1115 \exp\left(\frac{22.452T}{272.55+T}\right) \quad \text{(A.2)}$$

and

$$f_w = 1.0007 + (3.46 \times 10^{-6} P) \quad \text{(A.3)}$$

$$f_i = 1.0003 + (4.18 \times 10^{-6} P) \quad \text{(A.4)}$$

where e_w and f_w are the water vapor pressure and the enhancement factor over the surface of liquid water, respectively, while e_i and f_i are those over the surface of ice, respectively. Units are °C for temperature, T, and mb (=hPa) for pressure, P. f_w and f_i correct the differences of saturation vapor pressure between pure water vapor and moist air. This correction is a weak function of temperature and pressure, averaging f ~1.005 near sea level. However, in the manufacturer's calibration and in this study, the enhancement factor is set to f = 1. This approximation holds with an error 0.5% or less (WMO 2008).

Appendix B

We estimate the measurement uncertainties associated with this study by following the guidelines in JCGM/WG1 (2008).

First, we attempt to identify the likely sources of uncertainty and express them as a standard uncertainty.

In this study, the major elements of the conceivable uncertainties are from each instrument's performance, spatial and temporal non-uniformity in the chamber, and reading errors. The accuracy of the RF-100 is ±0.1°C according to the manufacturer's specifications. We assume that the true value exists within a rectangular ±0.1°C distribution. Consequently, the standard uncertainty of the reference temperature measurement u_{T0} becomes

$$u_{T0} = \frac{0.1}{\sqrt{3}} = 0.058^{\circ}\mathrm{C} \quad \text{(B.1).}$$

For the reference dew point sensor FDW10, the accuracy is ±0.5°C. The standard uncertainty of the reference dew point measurements is u_{m0}, which is

$$u_{m0} = \frac{0.5}{\sqrt{3}} = 0.29^{\circ}\mathrm{C} \quad \text{(B.2).}$$

To assess the uncertainty from the spatial and temporal non-uniformity in the PVC pipe, we measure the temperature and RH at three points within the pipe using the same RS-06G and obtain temperatures of +17.6°C, +17.7°C, and +17.7°C, and RH levels of 27.1%, 27.3%, and 27.1%, respectively. These RH values correspond to dew point temperatures of approximately −1.6°C, −1.4°C, and −1.5°C. Temporal fluctuations during measurement are small and steady and remain within ±0.02°C. Consequently, we assume that the spatial and temporal non-uniformity of temperature do not exceed 0.1°C; i.e., the air temperatures in the PVC pipe remain within a rectangular ±0.05°C distribution, and thus, the standard uncertainty u_{T1} becomes

$$u_{T1} = \frac{0.05}{\sqrt{3}} = 0.029^{\circ}\mathrm{C} \quad \text{(B.3).}$$

We assume that the uncertainty of the dew point temperatures due to the spatial and temporal non-uniformity would not exceed 0.2°C; i.e., the dew point temperatures in the PVC pipe remain within a rectangular ±0.1°C distribution; thus, the standard uncertainty u_{m1} becomes

$$u_{m1} = \frac{0.1}{\sqrt{3}} = 0.058^{\circ}\mathrm{C} \quad \text{(B.4).}$$

To estimate the reading errors, we complete five replicate readings for every condition and take their average as the measurement value. For temperature measurements, the standard uncertainties u_{T2} from the readings become

$$u_{T2} = \frac{s}{\sqrt{n}} = 0.029 \text{ to } 0.071^{\circ}\mathrm{C} \quad \text{(B.5)}$$

where s is the standard deviation, and n is the frequency of measurement (i.e., n = 5). For dew point measurements, the standard uncertainties u_{m2} from the readings become

$$u_{m2} = \frac{s}{\sqrt{n}} = 0.029 \text{ to } 0.13^{\circ}\mathrm{C} \quad \text{(B.6).}$$

Next, we determine the combined standard uncertainty from these three separate factors. The combined standard uncertainty of temperature measurement, u_T, is

$$u_T = \sqrt{u_{T0}^2 + u_{T1}^2 + u_{T2}^2} = 0.065 \text{ to } 0.096^{\circ}\mathrm{C} \quad \text{(B.7).}$$

The combined standard uncertainty of dew point measurement, u_m, is

$$u_m = \sqrt{u_{m0}^2 + u_{m1}^2 + u_{m2}^2} = 0.29 \text{ to } 0.32^{\circ}\mathrm{C} \quad \text{(B.8).}$$

Furthermore, we calculate the combined standard uncertainty of RH using the law of propagation of uncertainty. The combined standard uncertainty of RH, u_{RH}, is written as

$$u_{RH} = \sqrt{\left(\frac{\partial RH}{\partial T_a}\right)^2 u_T^2 + \left(\frac{\partial RH}{\partial T_m}\right)^2 u_m^2} = 0.36\% \text{ to } 1.7\% \text{ RH} \quad \text{(B.9).}$$

To determine expanded uncertainty, we use k = 2 as level of confidence. Thus, the expanded uncertainty of RH, U_{RH}, becomes

$$U_{RH} = k \times u_{RH} = 0.72\% \text{ to } 3.4\% \text{ RH} \quad \text{(B.10).}$$

The values of U_{RH} for each condition are shown in Fig. 3.

References

Buck, A. L. 1981: New equations for computing vapor pressure and enhancement factor. *J. Appl. Meteor.*, **20**, 1527–1532.

Houze, R., A., 1993: *Cloud Dynamics*. Academic Press, California, 573 pp.

Ibata, K., and Y. Kanai, 2008: Development of the micro chilled mirror hygrometer. *Proceedings of the 5th International Symposium on Humidity and Moisture*— ISHM 2006 Brazil.

Ishihara, M., 2004: Presentation on recent national tests/comparisons. Recent tests and comparisons of radiosonde operated by Japan Meteorological Agency. WMO commission for instruments and methods of observation, 8 pp. [Available online at http://www.wmo.int/pages/prog/www/IMOP/meetings/Upper-Air/Systems-Intercomp/Doc3-2(3).pdf.]

Joint Committee for Guides in Metrology/ Working Group 1, 2008: *Evaluation of measurement data—Guide to the expression of uncertainty in measurement*. JCGM, **100**, 134 pp. [Available online at http://www.bipm.org/utils/common/documents/jcgm/JCGM_100_2008_E.pdf.]

Murphy, D., and T. Koop, 2005: Review of the vapour pressures of ice and supercooled water for atmospheric applications. *Quart. J. Roy. Meteor. Soc.*, **131**, 1539–1565.

Miloshevich, L. M., H. Vömel, A. Paukkunen, A. J. Heymsfield, and S. J. Oltmans, 2001: Characterization and correction of relative humidity measurements from Vaisala RS80-A radiosondes at cold temperatures. *J. Atmos. Oceanic Technol.*, **18**, 135−156.

Miloshevich, L. M., A. Paukkunen, H. Vömel, and S. J. Oltmans, 2004: Development and validation of a time-lag correction for Vaisala radiosonde humidity measurements. *J. Atmos. Oceanic Technol.*, **21**, 1305−1327.

Morrissey, J. F. and F. J. Brousaides, 1970: Temperature-induced errors in the ML-476 humidity data. *J. Appl. Meteor.*, **8**, 805−808.

National Oceanic and Atmospheric Administration, National Aeronautics and Space Administration, and United States Air Force, 1976: *U. S. Standard Atmosphere*. U. S. Government Printing Office, Washington, D. C., 227 pp.

Sakota Y, K Naganuma, Y Hagiwara, N Inoue, and A Mita, 1999: RS-91 type rawinsonde. *Kisho Kenkyu Note*, **194**, 3−24 (in Japanese).

Schroeder, S. R., 2008: Adjusting archived radiosonde data using complete validated and inferred radiosonde metadata to compute unbiased atmospheric temperature and moisture trends. *20th Conference on Climate Variability and Change*, New Orleans, 4–5. [Available online at https://ams.confex.com/ams/88Annual/techprogram/paper_130838.htm.]

Shimizu K., T. Asanuma, K. Yamaguchi, and K. Yoshikawa, 2008: Upgraded Thermistor for Unbiased Measurements—Evaluation of New GPS Radiosonde RS-06G, IOM 97, Papers presented at the WMO technical Conference on Instruments and Methods of observation (TECO 2008). [Available online at http://www.wmo.int/pages/prog/www/IMOP/publications/IOM-96_TECO-2008/P1(09)_Shimizu_Japan.pdf.]

Sugidachi, T., 2011: Development of a balloon-borne hygrometer for climate monitoring. master's thesis at Graduate school of Environmental Science, Hokkaido University, 138 pp (in Japanese). [Available online at http://wwwoa.ees.hokudai.ac.jp/~takuji-sugi/doc/M-ron_all.pdf.]

Vömel, H., D. E. David, and K. Smith, 2007a: Accuracy of tropospheric and stratospheric water vapor measurements by the cryogenic frost point hygrometer: Instrumental details and observations. *J. Geophys. Res.*, **12**, D08305, doi:10.1029/2006JD007224.

Vömel, H., H. Selkirk, L. Miloshevich, J. Valverde-Canossa, J. Valdés, E. Kyrö, R. Kivi, W. Stolz, G. Peng, and J. A. Diaz, 2007b: Radiation dry bias of the Vaisala RS92 humidity sensor. *J. Atmos. Oceanic Technol.*, **24**, 953–963.

Wang, J., H. L. Cole, D. J. Carlson, E. R. Miller, K. Beierle, A. Paukkunen, and T. K. Laine, 2002: Corrections of humidity measurement errors from the Vaisala RS80 Radiosonde-Application to TOGA COARE data. *J. Atmos. Oceanic Technol.*, **19**, 981−1002.

Williams, S. L., and D. T. Acheson, 1976: Thermal time constants of U. S radiosonde sensors used in GATE. NOAA Tech. Memo. EDS CEDDA-7, 16 pp. [Available from U. S. Govt. Printing Office, Washington, DC 20402.]

World Meteorological Organization, 1995: Manual on Codes. WMO-No. **306**, 503 pp. [Available online at http://www.wmo.int/pages/prog/www/WMOCodes/Manual/WMO306_Vol-I-1-PartA.pdf.]

World Meteorological Organization, 2008: *Guide to Meteorological Instruments and Methods of Observation-Seventh edition*. WMO-No. **8** (2008 edition. Update in 2010), 716 pp. [Available online at http://www.wmo.int/pages/prog/www/IMOP/CIMO-Guide.html.]

World Meteorological Organization, 2011: WMO Intercomparison of high quality radiosonde systems Yangjiang, China. 12 July–3 August 2010, IOM 107, Nash, J., T. Oakley, H. Vömel, and LI Wei (eds.), 248 pp. [Available online at http://www.wmo.int/pages/prog/www/IMOP/publications/IOM-107_Yangjiang.pdf.]

Yoneyama K., M. Fujita, N. Sato, M. Fujiwara, Y. Inai, and F. Hasebe, 2008: Correction for radiation dry bias found in RS92 radiosonde data during the MISMO field experiment. *SOLA*, **4**, 13–16.